

Single-field inflation constraints from CMB and SDSS data

Fabio Finelli,^{1,2,*} Jan Hamann,^{3,†} Samuel M. Leach,^{4,5,‡} and Julien Lesgourgues^{6,7,8,§}

¹INAF/IASF Bologna, Istituto di Astrofisica Spaziale e Fisica Cosmica di Bologna, via Gobetti 101, I-40129 Bologna, Italy

²INFN, Sezione di Bologna, via Irnerio 46, I-40126 Bologna, Italy

³Department of Physics and Astronomy, University of Aarhus, Ny Munkegade, DK-8000 Aarhus C, Denmark

⁴SISSA, Astrophysics Sector, via Beirut 2-4, I-34151 Trieste, Italy

⁵INFN, Sezione di Trieste, I-34151 Trieste, Italy

⁶CERN, Theory Division, CH-1211 Geneva 23, Switzerland

⁷Institut de Théorie des Phénomènes Physiques, EPFL, CH-1015 Lausanne, Switzerland

⁸LAPTh (CNRS - Université de Savoie), BP 110, F-74941 Annecy-le-Vieux Cedex, France

(Dated: April 11, 2019)

We present constraints on canonical single-field inflation derived from WMAP five year, ACBAR, QUAD, BICEP data combined with the halo power spectrum from SDSS LRG7. Models with a non-scale-invariant spectrum and a red tilt $n_s < 1$ are now preferred over the Harrison-Zel'dovich model ($n_s = 1$, tensor-to-scalar ratio $r = 0$) at high significance. Assuming no running of the spectral indices, we derive constraints on the parameters (n_s , r) and compare our results with the predictions of simple inflationary models. The marginalised credible intervals read $n_s = 0.962^{+0.028}_{-0.026}$ and $r < 0.17$ (95% confidence level). Interestingly, the 68% c.l. contours favour mainly models with a convex potential in the observable region, but the quadratic potential model remains inside the 95% c.l. contours. We demonstrate that these results are robust to changes in the datasets considered and in the theoretical assumptions made. We then consider a non-vanishing running of the spectral indices by employing different methods, non-parametric but approximate, or parametric but exact. With our combination of CMB and LSS data, running models are preferred over power-law models only by a $\Delta\chi^2 \simeq 5.8$, allowing inflationary stages producing a sizable negative running $-0.063^{+0.061}_{-0.049}$ and larger tensor-scalar ratio $r < 0.33$ at the 95% c.l. This requires large values of the third derivative of the inflaton potential within the observable range. We derive bounds on this derivative under the assumption that the inflaton potential can be approximated as a third order polynomial within the observable range.

PACS numbers:

I. INTRODUCTION

Recent advances in centimetre and millimetre wave detector technology are ushering in an exciting observational window on the physics of the early universe. The celebrated ‘inflation’ model [1, 2] provides a compelling framework for thinking about conditions that might have prevailed in the early universe, yet to date there is no real consensus on what is the underlying inflationary model. A well-known implementation of the idea relies on scalar field models, for which the inflationary predictions can, nonetheless, be worked out in detail. Although it is sometimes claimed that inflation ‘can predict anything’, this view misses the point that, notwithstanding the impressive successes of the Wilkinson Microwave Anisotropy Probe (WMAP) [3], currently there is a real dearth of hard new facts relating to early universe physics, and that the predictions of inflation have yet to be put under any real strain.

As a consequence there is a need for continual moni-

toring of the parameters of a generic inflation model, as constrained primarily by measurements of Cosmic Microwave Background (CMB) anisotropies and surveys of the tracers of Large Scale Structure (LSS). Once the values of the parameters of inflation have been determined then the implications for the physics of inflation can be worked out. In the long term, it is possible that an improved understanding of the physics of inflation could put an important constraint on the physics of the early universe, just as an understanding of the physics of nucleosynthesis has for a long time been an important constraint on physics beyond the standard model of particle physics.

Some constraints on inflation incorporating WMAP five-year data (WMAP5) have been published by Komatsu et al. [4], Peiris & Easter [5] and Kinney et al. [6], using different combinations of WMAP, small-scale CMB data from ACBAR [7], Baryon acoustic oscillation (BAO) data from [8], or SNIa data from the Supernovae Legacy Survey [9]. Since then, some important new data sets have been released, like CMB polarisation measurements from BICEP [10] and QUAD [11], the galactic halo correlation function derived from Luminous Red Galaxies in the data release seven of the Sloan Digital Sky Survey (LRG7), and the luminosity distance of Type Ia supernovae (SNIa) from the SDSS-II survey [12]. These new data sets have been a stimulus to our anal-

*Electronic address: finelli@iasfbo.inaf.it

†Electronic address: hamann@phys.au.dk

‡Electronic address: leach@sissa.it

§Electronic address: julien.lesgourgues@cern.ch

ysis at a time when increasingly detailed measurements of the CMB from WMAP and Planck [13], as well as a number of sub-orbital experiments such as ACT [14], SPT [15], QUIET [16], SPIDER [17], PolarBear [18] and EBEX [19], are expected over the course of the next couple of years.

In this work, we will use a combination of the most up-to-date CMB data and of the LRG7 halo correlation function for updating constraints on single-field inflationary models. After discussing our methodology in Section II, we present a discussion of the status of the Harrison-Zel'dovich model in Section III, which is the simplest possible empirical model for primordial perturbations. Then, in Section IV, we show our results for the simplest class of inflationary models, those that do not lead to any significant running of the tilt in the scalar primordial spectrum. In Section V, we take a more conservative point of view of deriving constraints on the observable part of the inflaton potential using different methods (non-parametric but approximate, or parametric but exact). Our conclusions are summarized in Section VI.

II. METHODOLOGY

We perform an analysis of the WMAP [20, 21], ACBAR [7], BICEP [10] and QUaD [11] CMB anisotropy data, combined with the LRG7 halo correlation function computed in [22, 23]. In order to avoid correlations between different data sets which cover the same region of the sky, we removed from the analysis a few CMB band powers, specifically a) all the QUaD TT band powers since they overlap with data from the ‘CMB8’ region of ACBAR, b) the ACBAR band powers with $\ell < 790$ and $\ell > 1950$ to avoid overlap with WMAP (which is cosmic variance limited up to $\ell = 530$ [20]) and contamination from foreground residuals, respectively, c) the QUAD TE band powers which overlap with WMAP ones, the QUAD EE band powers which overlap with BICEP, d) the BICEP TT, TE band powers (i.e., we use just EE and BB information from BICEP). Unless otherwise specified, all the results of this paper are derived from this combination of data. In some particular cases, we also considered the impact of ancillary data such as the recent determination of the Hubble constant $H_0 = 74.2 \pm 3.6 \text{ km s}^{-1} \text{ Mpc}^{-1}$ by Riess et al. [24], and the luminosity distance of SNIa from [12].

We use CosmoMC [25, 26] in order to compute the Bayesian probability distribution of model parameters. The pivot scale of the primordial scalar and tensor power spectra was set to $k_* = 0.017 \text{ Mpc}^{-1}$, as recommended by [27], and we have verified that this choice of pivot scale is still close to optimum for the combination of data used in our analysis (see Section V). Apart from the primordial spectrum parameters (or inflationary parameters) described in the next section, we vary the baryon density $\omega_b = \Omega_b h^2$, the cold dark matter density $\omega_c = \Omega_c h^2$, the Hubble parameter $H_0 = 100h \text{ km s}^{-1} \text{ Mpc}^{-1}$ and the

reionisation optical depth τ . We assume a flat universe, and so the cosmological constant for each model is given by the combination $\Omega_\Lambda = [1 - (\omega_b + \omega_c)h^{-2}]$. We also assume a CMB temperature $T_{\text{CMB}} = 2.725 \text{ K}$ [28] and three neutrinos with a negligible mass (excepted in subsection IV D). We set the primordial helium fraction to $y_{\text{He}} = 0.248$, a value consistent with the predictions of standard Big Bang Nucleosynthesis for a baryon density of $\omega_b \simeq 0.0022$.¹ In order to fit WMAP, ACBAR and QUaD data, we use the lensed CMB and matter power spectra and we follow the method implemented in CosmoMC consisting in varying a nuisance parameter A_{SZ} which accounts for the unknown amplitude of the thermal SZ contribution to the small-scale CMB data points assuming the model of [31]. We use a CAMB accuracy setting of at least 1.2. We sample the posterior using the Metropolis-Hastings algorithm [32] at a temperature $T = 2$ (for improved exploration of the tails), generating eight parallel chains and imposing a conservative Gelman-Rubin convergence criterion [33] of $R - 1 < 0.01$.

III. DISCUSSION OF HZ MODEL

The empirical model for the spectrum of primordial perturbations proposed by Harrison [34], Zel'dovich [35] and Peebles [36] (hereafter the HZ spectrum) has a single parameter describing primordial perturbations, namely the primordial spectrum amplitude A_S . It is interesting to compare its goodness-of-fit with the next-level model in terms of number of free parameters, namely a model with a power-law primordial spectrum with tilt n_s but no tensor perturbations (this model can be motivated by low-scale slow-roll inflation). The general mood is that with the increasing precision of CMB anisotropy measurements, the HZ spectrum is on the verge of being ruled out in favour of a model with a red tilt.

However, keeping an open mind about the origin of primordial perturbations, the HZ spectrum still holds an allure as a possible indicator of to-be-discovered symmetries of the early universe. As a result we have taken a slightly different tack by assuming for a moment that the HZ spectrum is not only a viable but a correct description of the data, thereby reducing the dimensionality of the parameter space, in order to examine in detail some of the cracks in this model that are beginning to appear. Using our basic data set (WMAP5, ACBAR, BICEP, QUaD and LRG7) we ran MCMC chains for the HZ model and for the tilted model. Introducing a tilt decreases the minimum effective chi square by $\Delta(-2\ln(\mathcal{L})) = 12.6$,

¹ Under the assumptions of standard BBN, the commonly used value of $y_{\text{He}} = 0.24$ corresponds to $\omega_b \sim 0.01$, which is clearly inconsistent with observations. With the rather modest sensitivity of present data to y_{He} [29], this choice may not lead to significant bias, but for data from the Planck satellite the issue will become relevant [30].

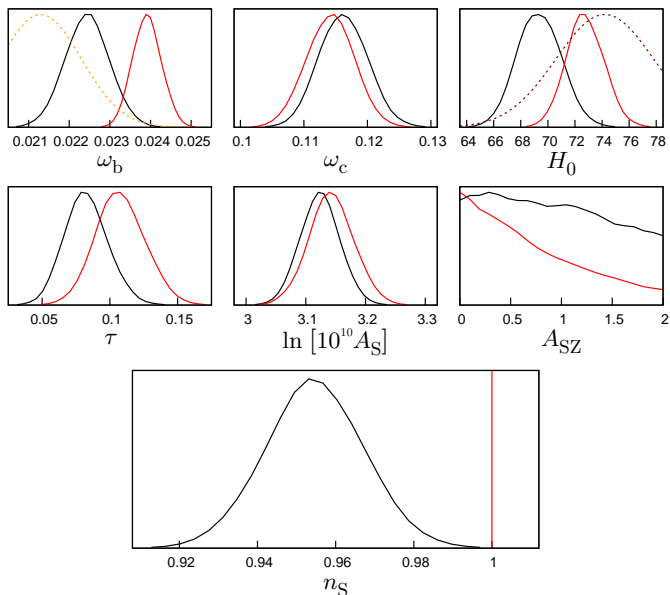


FIG. 1: Posterior probabilities of the parameters of the HZ model (red) and the tilted model (black). The dotted orange line denotes constraints on ω_b from BBN and the dotted maroon line represents the HST prior on H_0 .

which clearly implies a tension between the HZ model and the data². On top of that, the HZ model also leads to different preferred ranges for the cosmological parameters, as can be checked from Figure 1 and Table I. In particular, fixing $n_S = 1$ implies a rather high baryon density of $\omega_b = 0.0239 \pm 0.0007$ (at 95% c.l.), which is at odds with recent constraints from measurements of primordial element abundances within the standard Big Bang Nucleosynthesis scenario. Indeed, a conservative bound based only on the deuterium abundance yields $\omega_b = 0.0213 \pm 0.002$ (at 95% c.l.) [39]. The statistical error shrinks by a factor two when ^4He measurements are included [40]. Taking the deuterium bound on ω_b as a prior yields $\Delta(-2\ln(\mathcal{L})) = 17.6$ – a difference exceeding the 4σ level. We conclude that the HZ model is now clearly incompatible with CMB and LSS data under the

	HZ	tilted
ω_b	0.0239 ± 0.0007	0.0224 ± 0.001
ω_c	0.114 ± 0.007	0.116 ± 0.007
h	$0.728^{+0.027}_{-0.026}$	$0.694^{+0.032}_{-0.030}$
τ	$0.108^{+0.036}_{-0.034}$	$0.083^{+0.032}_{-0.029}$
$\log [10^{10} A_S]$	3.14 ± 0.07	3.12 ± 0.06
n_S	–	$0.955^{+0.024}_{-0.026}$
σ_8	0.853 ± 0.048	$0.822^{+0.047}_{-0.045}$

TABLE I: Mean parameter values and bounds of the central 95%-credible intervals for the HZ model and the tilted model.

assumption of the standard ΛCDM cosmology.

We remark that the HZ model also implies a value of the baryon fraction $f_b \equiv \omega_b/(\omega_b + \omega_c) = 0.173 \pm 0.005$ (at 68% c.l.) which is about a percent higher than the corresponding value in the n_S model which implies $f_b = 0.162 \pm 0.005$ (at 68% c.l.). It appears though that, notwithstanding observational uncertainties of the total mass of clusters and theoretical uncertainties in the physics of feedback in clusters, the slightly higher value of the baryon fraction in the HZ model can easily be accommodated by the most recent X-ray observations of clusters (see for instance [41]). This result merely highlights the current, but rather mild, model dependence of the baryon fraction.

Finally we note from Figure 1 that the preferred value of A_{Sz} is zero, which results from the fact that both n_S and A_{Sz} change the ratio of large-scale to small-scale power in the C_ℓ . Taken at face value this is arguably another point against the HZ model. On the other hand the HZ model does prefer a value of H_0 that is slightly more consistent with value of $H_0 = 74.2 \pm 3.6 \text{ km s}^{-1} \text{ Mpc}^{-1}$ from [24].

To summarise this section, we have argued that the HZ model faces pressure both on grounds of goodness of fit, but also on grounds of poor astrophysical consistency. As mentioned later in section IV D, the inclusion of neutrino masses would not alleviate the pressure on the HZ model.

IV. CONSTRAINTS ON THE SIMPLEST MODELS OF INFLATION

A. Motivations

Most inflationary model discussed in the literature lead to a power-law scalar spectrum, i.e., to a negligible running of the scalar tilt. This follows from a well-known argument which can be summarised in the following way. The function accounting for the Hubble parameter as a function of the field (or as a function of the number of e -folds) can be expanded around any value in an infinite hierarchy of slow-roll parameters ϵ_n , each one accounting for the logarithmic derivative of the previous term ϵ_{n-1} (see for instance [42, 43, 44] or Appendix B). Current bounds on the tensor-to-scalar ratio r and scalar tilt n_S imply that the first two parameters ϵ_1 and ϵ_2 are much

² While this work was being completed, Refs. [37, 38] appeared and addressed this issue more specifically with different methods. In Ref. [37], the Bayesian evidence ratio between the HZ and power-law models is computed for a data set slightly different from ours, using a prior $0.8 < n_S < 1.2$ for the power-law model. The authors conclude that there is strong negative evidence for the HZ model. In this paper we do not quote an evidence ratio because this would require a very good sampling of the distribution tail for $\mathcal{P}(n_S)$ in the power law model, four sigma away from the maximum, and our runs were not designed for this purpose. Instead, Ref. [38] proposes a method for reconstructing the primordial scalar spectrum with no underlying theoretical or inflationary prior. The conclusion of this work is still that a scale-invariant spectrum is disfavored, but only weakly (consistently, when theoretical priors are removed, one reaches more conservative conclusions).

smaller than one, as expected during slow-roll inflation. So, a sizeable running α_S on observable scales can only be generated when one of the parameters ϵ_n with $n \geq 3$ is roughly of order one or larger when observable scales leave the Hubble radius during inflation, i.e. when some derivatives of the first two slow-roll parameters are very large. If this is not the case, the running will be of the order of $\epsilon_1 \epsilon_2$, i.e. at most of the order of $\alpha_S \sim \mathcal{O}(10^{-4})$.

On the other hand, the number of e -folds required between that time and the end of inflation (which depends on the scale of inflation, on the details of inflation ending, and on the efficiency of the reheating mechanism) can be conservatively assumed to lie in the range from 30 to 60 e -folds. For any smooth potential, a sizeable running $|\alpha_S| > 0.01$ implies such large derivatives of the first two slow-roll parameters in the observable range that inflation would end very few e -folds after galaxy scales leave the Hubble radius, not even reaching 30 inflationary e -folds [45, 46]. This argument can only be evaded: (i) with very special potentials (incorporating sharp features, or such that their Taylor-expansion involves very high-order coefficients, see for instance [45, 47, 48]); (ii) within set-ups involving several inflaton fields, leading to a phase transition or even to several short stages of inflation, such that the required 30 to 60 inflationary e -folds are not contiguous. Since these situations are beyond minimal requirements, and since the sensitivity of current data to running ($\Delta\alpha_S \sim \mathcal{O}(10^{-2})$) is far too small for probing generic slow-roll model predictions ($\alpha_S \sim \mathcal{O}(10^{-4})$), it appears sensible to perform an analysis where the running is assumed to be negligible, in order to preserve the simplicity of the inflationary paradigm. We will relax this theoretical prejudice in the next section.

We thus consider all inflationary models which can be described by the primordial perturbation parameters consisting of the scalar amplitude and spectral index (A_S, n_S), and the tensor-to-scalar ratio r (both defined at the pivot scale $k_* = 0.017 \text{ Mpc}^{-1}$). In single-field inflation, deep in the slow-roll limit, the tensor spectrum shape is not independent of the scalar one. We will consider a tensor spectrum with a tilt $n_T = -r/8$, as predicted for canonical single-field inflation at first-order in slow-roll.

B. Results for the basic data set, and implications for inflation

In Table II, we present constraints on each parameter of this model, using only CMB data in the first column, and our reference data set (CMB plus LRG7) in the second one. In Figure 2 we focus on the joint probability in the (n_S, r) plane, for the reference data set. Compared to the results obtained by [4], our constraints are shifted towards slightly lower tilts and significantly lower tensor-to-scalar ratios. The marginalised 95%-credible interval for the tilt is given by $n_S = 0.962^{+0.028}_{-0.026}$ (to be compared with the result of the previous section, $n_S = 0.955^{+0.024}_{-0.026}$,

	CMB only	CMB+LRG7	CMB+BAO
ω_b	$0.0230^{+0.0013}_{-0.0012}$	0.0227 ± 0.0011	0.0226 ± 0.0011
ω_c	$0.105^{+0.012}_{-0.013}$	$0.115^{+0.008}_{-0.007}$	0.113 ± 0.007
h	$0.746^{+0.066}_{-0.056}$	$0.700^{+0.034}_{-0.032}$	0.708 ± 0.030
τ	$0.091^{+0.036}_{-0.034}$	$0.083^{+0.033}_{-0.029}$	$0.085^{+0.033}_{-0.030}$
$\log [10^{10} A_S]$	3.08 ± 0.08	$3.12^{+0.06}_{-0.07}$	$3.11^{+0.07}_{-0.06}$
n_S	$0.975^{+0.039}_{-0.031}$	$0.962^{+0.028}_{-0.026}$	$0.961^{+0.027}_{-0.026}$
r	< 0.29	< 0.17	< 0.18

TABLE II: Mean parameter values and bounds of the central 95%-credible intervals for the parameters of the vanilla+ r model and various combinations of data sets. For the tensor-to-scalar ratio r the 95%-credible upper bound is quoted.

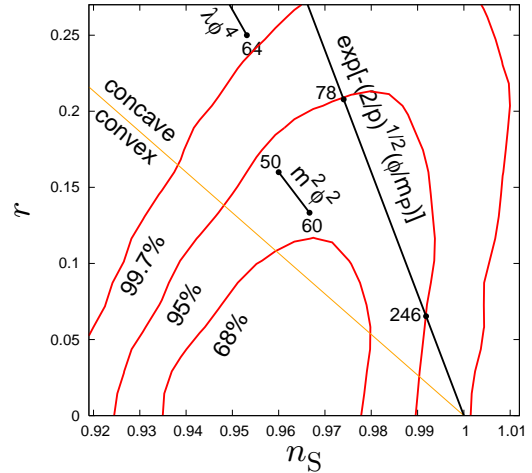


FIG. 2: Marginalised joint 68%-, 95%- and 99.7%-credible contours in the (n_S, r) plane for our reference data set (CMB plus LRG7). The orange line shows the limit between inflationary models with a concave/convex potential in the observable range. We show in black the regions corresponding to popular concave models with a quadratic, quartic or exponential potential.

obtained for low energy scale inflationary models with $r \simeq 0$). At the same confidence level, our result for the tensor-to-scalar ratio is $r < 0.17$. This corresponds to an upper bound on the energy scale of inflation

$$V_* = \frac{3A_S r m_P^4}{128} < 8.9 \times 10^{-12} m_P^4 = (2.1 \times 10^{16} \text{ GeV})^4$$

at 95% c.l., where $m_P = G^{-1/2}$ stands for the Planck mass (the reduced Planck mass, referred to in the next sections, will be denoted as $M_P = (8\pi G)^{-1/2}$). Bounds on quantities which are not sharply constrained by the data, like r or V_0 , depend mildly on the choice of parametrisation, as illustrated in [49], but for reasonable choices this will not affect our qualitative conclusions.

As pointed out in previous works (see for instance [4, 6]), current data mainly raise some tension for inflationary models with a concave potential. Most of the 68% allowed region lies below the convex potential limit, and convex models with a red tilt in the range [0.93-0.99] are comfortably allowed by the data. These include for

instance:

- ‘Natural inflation’ [50] with the potential $V(\phi) = \Lambda^4 [1 + \cos(\phi/f)]$ leading to the prediction $n_S \simeq 1 - m_P^2/(8\pi f^2)$, which is allowed only for $f > 0.73 m_P$ (95% c.l.).
- More generally, ‘new inflation’ type models where the inflaton rolls away from unstable equilibrium with a slope given by $V(\phi) = V_0[1 - (\phi/\mu)^\alpha]$. For $\alpha = 2$ and assuming $|\phi| \ll \mu$ when observable scales leave the Hubble radius, our constraints imply $1.5 < \mu/m_P < 4.0$ (95% c.l.). Inflationary models with $\alpha \geq 3$ are all in good agreement with observations.
- ‘Hybrid inflation’ with a logarithmic slope (caused for instance by one-loop corrections during global SUSY inflation [51]), which predicts a small r and n_S close to 0.98.
- Inflationary models predicting a red tilt for scalar perturbations and a tensor-to-scalar ratio $\sim \mathcal{O}((n_S - 1)^2)$, as $R + R^2/(6M^2)$ [1] or Standard Model Higgs inflation [52], are in good agreement with observations.

Among concave models, we can single out a few generic models for further discussion:

- Inflation with a quadratic potential $V = \frac{1}{2}m^2\phi^2$ (often dubbed ‘chaotic inflation’ after Ref. [53]) lives along the line $r \simeq -4(n_S - 1)$ during slow-roll. The position of the model along this line depends on the number of e -folds N_* between the time of Hubble crossing for the pivot scale, and the end of inflation. In turn, this number depends on the reheating temperature. Due to uncertainties on the reheating stage, we consider here a plausible range $50 < N_* < 60$, for which quadratic inflation is still within the 95%-credible region in the (n_S, r) plane, as can be seen in Figure 2. Note that updated constraints on the mass can be inferred from the combination $(3A_S)^{1/2}/(2N_*)$ which is equal to (m/m_P) in this model. Varying A_S in the 95%-credible range given by Table II, and N_* between 50 and 60, we find that the mass of chaotic inflation models lies in the range from $6.6 \times 10^{-7}m_P$ to $8.5 \times 10^{-7}m_P$.
- Inflation with a quartic potential $V = \lambda\phi^4/4$ lives along the line $r = -16/3(n_S - 1)$ during slow-roll. For this model, there are indications that the number of e -folds N_* should be increased by four, for the reasons summarised in [54]. In Figure 2 we show the line corresponding to quartic inflation for $N_* < 64$. This model is found to be outside of the 99.7%-credible region in the (n_S, r) plane.
- Inflation with an exponential potential $V = \exp[-\sqrt{p/2}(\phi/M_P)]$ is called power-law inflation

[55], because the exact solution for the scale factor is given by $a(t) \propto t^p$. This model is incomplete, since inflation would not end without an additional mechanism which stops it. Assuming that such a mechanism exists and leaves unmodified its predictions on cosmological perturbations, we can constrain this model since it predicts $r = -8(n_S - 1)$ and $n_S = 1 - 2/(p - 1)$. Only models with $78 < p < 246$ are found to lie within our 95%-credible region in the (n_S, r) plane.

- Hybrid or ‘false-vacuum’ inflation with a quadratic slope and an effective potential $V = V_0 + \frac{1}{2}m^2\phi^2$ is also compatible with the data provided that V_0 is not too large with respect to the quadratic term. In this model, the two slow-roll parameters are related through $\alpha\eta^2 + \epsilon - \eta = 0$, where $\alpha \equiv 8\pi V_0/(m^2 m_P^2)$. For $\alpha < 80$ this relation is not compatible with our 95%-credible region in (n_S, r) space. We conclude that independently of the mechanism responsible for the end of hybrid inflation, this class of models should obey to the constraint $V_0 \leq 3m^2 m_P^2$. Note however that this model is usually invoked as a way to obtain $|\phi_*| \ll M_P$, and to avoid large radiative corrections during inflation [56]. This can be achieved when the term V_0 dominates over the quadratic one, i.e. in the large α limit – a situation constrained by current data.

C. Impact of extra data sets

1. Baryon acoustic oscillations

The results presented in the third column of Table II show that the constraints on the primordial spectrum parameters do not degrade significantly if we replace the LRG7 power spectrum by constraints on the baryon acoustic oscillation scale derived from the same survey data [57]. This is a clear indication that the shape information contained in the galaxy power spectrum data is not very relevant here – the improvement over the results from a CMB only analysis stems entirely from the geometrical information; it also implies that our estimates are unlikely to be affected by uncertainties in the modeling of non-linear structure growth at small scales.

2. Supernova luminosity distances

Even though the luminosity distances of type Ia supernovae are not a direct probe of the primordial perturbations, their ability to constrain the expansion history of the low-redshift universe may still contribute useful information about inflation by helping alleviate parameter degeneracies in the model. The most recent compilation of SN data was presented by Kessler et al. [12], who give two different sets of luminosity distances, derived from

the same observations, but using either the MLCS2K2 or SALT-II lightcurve-fitting algorithms. In order to test whether SN add any useful information to our analysis of inflationary parameters we have separately combined the two luminosity distance data sets with the CMB+LRG7 data. In Figure 3 we plot the resulting constraints in the (n_s, r) plane. The discrepancy between the results for the two light curve fitters is evident, and has already been pointed out in Ref. [12] in the context of the dark energy equation of state parameter. Whereas adding the SALT-II data has no appreciable effect on our n_s and r constraints, the MLCS2K2 data would lead to a significantly tighter bound on the tensor-to-scalar ratio. This effect can be traced back to MLCS2K2's apparent preference for large values of Ω_m . Given that at the moment the SN data fail a basic self-consistency test between different methods, we choose to refrain from combining them with the more robust CMB+LRG7 data in the following sections.

3. Direct constraints on the Hubble parameter

We studied the impact of imposing the recent determination of H_0 from the measurement of nearby supernovae with the Hubble Space Telescope [24], which corresponds closely to $H_0 = 74.2 \pm 3.6 \text{ km s}^{-1} \text{ Mpc}^{-1}$ for the Λ CDM cosmology (we verified that ‘post-processing’ the Markov chains with a Gaussian prior on H_0 yields virtually identical results to those obtained using the weakly cosmology dependent H_0 likelihood code provided by [8] and included in the October 2009 version of CosmoMC). We found that since CMB+LRG7 prefer a slightly lower value of H_0 at 1σ , then imposing the H_0 constraint shifts ω_B and hence n_s to slightly larger values.

D. Impact of neutrino masses

In this subsection, we address the probably most well-motivated extension of the basic cosmological model, massive neutrinos. In [58], the inclusion of a neutrino mass parameter was shown to weaken parameter constraints on n_s and r enough to affect conclusions about the $\lambda\phi^4$ model of inflation in particular, mainly due to a parameter degeneracy with r . Interestingly we find that the more recent data effectively break this degeneracy: the constraints for the vanilla+ r + m_ν model in the (n_s, r) plane are essentially identical to the ones of the massless neutrino model, see top right panel of Figure 3. We find an upper limit on the sum of neutrino masses of $\sum m_\nu < 0.64 \text{ eV}$ (at 95% c.l.), consistent with the results of a recent analysis with similar data sets [59]. One might also wonder whether the presence of massive neutrinos could help alleviate the problems of the HZ model by virtue of the free-streaming-induced suppression of the matter power spectrum at small scales. This does not happen to be the case here, however; neither the baryon

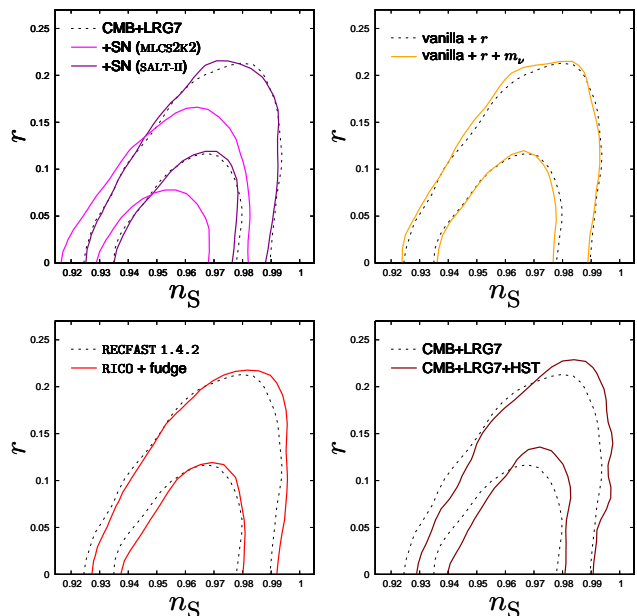


FIG. 3: Marginalised joint 68%- and 95%-credible contours in the (n_s, r) plane, illustrating the impact of various systematic effects. The dotted black lines represent the results of our ‘default’ setup in all three plots and are identical to the contours presented in Figure 2.

Top left: Results for CMB+LRG7 data alone, and combined with luminosity distances from the supernova compilation of Ref. [12], analysed with the MLCS2K2 (solid purple lines), and SALT-II (solid pink lines) lightcurve fitters.

Top right: Comparison of results for the massless neutrino and massive neutrino (orange lines) cases.

Lower left: CAMB’s default recombination code RECAST 1.4.2 compared to recombination calculated with RICO, including a ‘fudge function’ which accounts for corrections due to Raman scattering and Ly- α radiative transfer effects (red lines).

Lower right: Results for CMB+LRG7 compared to CMB+LRG7 combined with the H_0 measurement from [24] (solid maroon lines).

density nor the spectral index are significantly shifted with respect to the massless neutrino model.

E. Impact of recombination uncertainties

One of the remaining major theoretical uncertainties in the calculation of CMB angular power spectra is the physics of recombination. The standard approach relies on an effective description of hydrogen recombination assuming a 3-level hydrogen atom, as implemented in the widely-adopted RECAST code [60, 61], whose latest version 1.4.2 [62, 63], is the default model used in CAMB. The authors of RECAST estimate that the computed ionisation fraction $x_e(z)$ is accurate at the percent level. However, any error in $x_e(z)$ will inevitably propagate to the C_ℓ s, affecting in particular the small scales, and can potentially lead to biased parameter estimates.

Recently, there has been a lot of progress in under-

standing the physics of recombination (see for instance Refs. [64, 65]), and it seems that the accuracy required for Planck-quality data has now been reached. The results of the latest state-of-the-art recombination calculations can be implemented in a parameter estimation analysis with the help of RICO [66], an interpolation code for $x_e(z)$. In order to estimate the bias from recombination errors on the inflation-related parameters, we performed an analysis with RICO (including a ‘fudge function’ accounting for corrections due to Raman scattering and Ly- α radiative transfer effects, see Figure 1 of Ref. [64]) instead of RECFAST.

Our results are shown in the bottom panel of Figure 3; the credible regions in the (n_s, r) plane are shifted slightly towards bluer tilts, though not at an alarming level. We confirm the conclusion of Ref. [64] that for present data, the current version of RECFAST is sufficiently accurate.

V. CONSERVATIVE CONSTRAINTS ON THE OBSERVABLE INFLATON POTENTIAL

A. Motivations

The results of the previous section assume a negligible running of the scalar and tensor tilts. Indeed, these runnings are completely generic in inflation, but typically as small as $\alpha_s \sim \mathcal{O}(10^{-4})$ for the simplest slow-roll models, as already stated in Section IV. In other words, we implicitly supposed in Section IV that the inflaton rolls down a smooth potential well satisfying the slow-roll conditions and providing enough inflationary e -folds for matching on to the post-inflationary expansion era. These assumptions maximise the beauty and simplicity of the inflationary paradigm. However, nature sometimes prefers some degree of complexity, and in principle inflation could take place along a complicated potential, or in a multi-dimensional field space, or in several stages associated to distinct mechanisms. Even in that case, inflation remains a key ingredient in the cosmological evolution, necessary to solve the flatness and horizon problems and to generate primordial perturbations. If we take the point of view of studying what the data really tells us on the inflaton potential (with the only assumption that when cosmological scales leave the Hubble scale, inflation is driven by a single scalar field with a canonical kinetic term), the best we can do is to measure the primordial spectrum or the underlying inflaton potential within the region probed by cosmological observations, with no attempt to extrapolate beyond that range.

It is sometimes argued that fitting the data with a large running in the scalar spectrum (of the order of $\alpha_s \sim \mathcal{O}(10^{-2})$ or more) is not consistent with the inflationary paradigm, because – as already argued in section IV A – such a large running signals that inflation ends soon after observable scales leave the Hubble radius. It is worth clarifying this argument. Of course, as long as

the purpose is to constrain inflation self-consistently, one should check that any large running model providing a good fit to the data is indeed compatible with the assumption that the expansion is accelerated as long as observable scales leave the Hubble radius. If this is the case, such a model cannot be eliminated without invoking some criteria of simplicity. Indeed, the observable part of the potential can always be extrapolated in such way to accommodate an arbitrary number of e -folds. For models with a large tilt running in the scalar spectrum, the *simplest* extrapolation schemes would suggest that inflation ends soon after cosmological scales leave the Hubble scale, but it is always possible to design the potential (i.e. to introduce enough derivatives) in order to extend the duration of inflation as desired. Alternatively, and as already mentioned in section IV A, it is always possible to stick to the assumption that the potential is smooth and inflation ends very quickly, provided that later on, one or several extra inflationary stages (associated with other inflatons) sum up to the desired 30 to 60 e -folds of accelerated expansion. This situation can even be argued to be generic in some particle physics frameworks see e.g. [67]).

B. Methods

The shape of the inflationary potential within the observable region can be constrained through various approaches that make accurate inflationary predictions:

- The scalar primordial spectrum can be Taylor-expanded at various orders (including a running of the tilt, a running of the running, etc.). Then, the free parameters of the model consist of the scalar spectrum amplitude, its various logarithmic derivatives at the pivot scale, and the tensor-to-scalar ratio. For consistency, the tensor spectrum shape should be fixed by the hierarchy of self-consistency conditions truncated at some order (see Appendix A). The data are used to provide constraints on these parameters ($A_s, n_s, \alpha_s, \dots, r$). A posteriori, these constraints can be converted into constraints on the scalar potential derivatives (or on combinations of these derivatives called the ‘potential slow-roll parameters’) by making use of some analytical formula valid at a given order in slow-roll (with the caveat that slow-roll can be marginally satisfied in this context). This approach was chosen for instance by [4].
- One can choose a parametrisation of $V(\phi)$ in the observable range (if the ‘observable potential’ is assumed to be smooth, a Taylor expansion is adequate). For each potential parameter set, the primordial spectra can be computed analytically or numerically and the model can be fitted to the data. In this case, the data provide direct constraints on the potential parameters, without relying on any

slow-roll expansion in the case of a numerical computation. The result depends on the initial value of $\dot{\phi}$. However, if one does not assume that inflation started just before the observable region is crossed, there is a unique choice for $\dot{\phi}$, corresponding to the inflationary attractor solution in phase space. This approach can be easily followed by making use of the `CosmoMC` inflation module³ released together with [68]. This module performs a fully numerical, accurate and fast computation of the primordial spectra, based on the integration of background and perturbation equations during inflation (see Appendix C).

- In order to relax the assumption on $\dot{\phi}$, one can perform a similar analysis targeting the function $H(\phi)$ instead of $V(\phi)$. Since each $H(\phi)$ corresponds to a unique $V(\phi)$, this method is equally appropriate for constraining $V(\phi)$, and naturally incorporates models for which inflation starts just before entering the observable region. This approach was followed in [5, 44, 46, 69, 70, 71], with various analytical or semi-analytical schemes for the calculation of the primordial spectrum (based on an expansion of $H(\phi)$ into Hubble Slow-Roll (HSR) parameters). It was also followed in [72, 73, 74] with a numerical calculation of the spectrum for Taylor-expanded functions $H(\phi)$. Although reconstructing $H(\phi)$ is slightly more general than $V(\phi)$, we will not follow this approach in the current paper because constraints obtained directly on the potential parameters (for instance on V'/V instead of H'/H^2) are slightly more convenient and suggestive for inflationary model-building.
- One can try to reconstruct the function $H(N)$ where $N = \ln a$ is the number of e -folds, using its expansion in Horizon Flow Functions (HFFs) evaluated at the time N_* when the pivot scale crosses the Hubble radius during inflation. Combinations of the first three HFFs at the pivot scale can be related to the primordial spectra using the second-order slow-roll approximation [43]. The same approximation also provides relations with the derivatives of the inflaton potential (see Appendix B). This approach was chosen in many papers, for instance [75, 76, 77].

In this work, we will mainly compare the first and second approaches, although including also the fourth one for comparison. Hence, we will first fit the data with primordial spectra described by the set of parameters (A_S, n_S, α_S, r) , and use second-order slow-roll formulae to translate our results either in terms of convenient combination of the potential parameters (V, V', V'', V''') , or

in terms of the HFF parameters. Next, we will check whether these results agree with a direct reconstruction of the HFF parameters (using the second-order slow-roll approximation to relate HFF parameters with the primordial spectra). Finally, we will relax any slow-roll assumption and constrain directly the same quantities using the numerical module of [68], assuming that the observable potential $V(\phi)$ can be described by an order two or three Taylor-expansion.

C. Results

1. Flat priors on the spectral parameters including running

We first run `CosmoMC` with flat priors on the spectral parameters $(\ln A_S, n_S, \alpha_S, r)$. For each parameter, the mean values and marginalised bounds on the central 95%-credible interval are given in Table III for three cases: with CMB data only, with our default dataset CMB+LRG7, and for the same dataset when r is kept fixed to zero (low-scale inflation limit). As in previous papers on the subject (see for instance [68, 77]), a large negative running is preferred, since the value $\alpha_S = 0$ is always above the 95%-credible interval. Adding the LRG7 data leads to a slightly smaller mean value $\alpha_S = -0.063$, but does not increase the level of significance at which running spectra are preferred. With the CMB+LRG7 data set, introducing a running decreases the minimum effective chi square by $\Delta(-2 \ln \mathcal{L}) = 5.8$, showing that a non-zero running is preferred by the data, but not with a high degree of significance⁴ (we recall that between the HZ and power-law model the effective chi square decreases by twice the same amount). In Figure 4 (red curves), we show the marginalized likelihood contours for two-dimensional projections of the parameter space (n_S, α_S, r) . As usual, the running is found to be slightly correlated with the tensor-to-scalar ratio, and for large values of r the data are compatible with more running. However, in the small-scale inflation limit (i.e. when we fix $r = 0$), running is preferred with roughly the same level of significance as in the $r \neq 0$ model, since in that case we find $\alpha_S = -0.046^{+0.038}_{-0.039}$ at the 95% level.

In the running model, the constraint on r degrades by a factor 2 with respect to the power-law model. The allowed range for n_S enlarges by a factor 1.5, but the mean value remains identical. Indeed, we choose our pivot scale at $k_* = 0.017 \text{ Mpc}^{-1}$ in order to remove most of the degeneracy between n_S and α_S , as can be checked in Figure 4.

⁴ While this work was being completed, Ref. [37] appeared, based on a slightly different data set. By computing the ‘Bayesian evidence’ ratio between the running and power-law models (with a top-hat prior on α_S in the range $[-0.1, 0.1]$), this analysis concludes that ‘running is not disfavored by the data nor required in modeling the data’.

³ <http://www.lapp.in2p3.fr/~valkenbu/inflationH/>

2. Flat priors on combinations of the HFFs at the pivot scale

Next, for comparison, we run `CosmoMC` with flat priors on combinations of the first three HFFs evaluated at the pivot scale, namely ϵ_1 , ϵ_2 and $\epsilon_2\epsilon_3$ (see Appendix B for definitions). We use the second-order slow-roll approximation in order to relate these parameters to the spectral parameters (n_S, α_S, r) . In Figure 5, we show our marginalized likelihood contours in two-dimensional projections of the parameter space $(\epsilon_1, \epsilon_2, \epsilon_2\epsilon_3)$. In Figure 4, we compare our results with those of the previous subsection, both expressed in the space of spectral parameters. Clearly, the ensemble of models covered by the two parametrisations is the same, and differences might be expected only due to different priors. However, the contours of the two runs overlap perfectly. This is an indication that in the range of models allowed by the data, the expressions for (n_S, α_S, r) in terms of $(\epsilon_1, \epsilon_2, \epsilon_2\epsilon_3)$ are dominated by linear terms, so that flat priors on one parameter set are nearly equivalent to flat priors on the other one. The run of this section does not bring new information on inflationary models but provides a useful self-consistency check.

Our constraints on the HFFs evaluated at the pivot scale are best summarized by

$$\begin{aligned} \epsilon_1 < 0.021, \quad \epsilon_2 + 2.7\epsilon_1 &= 0.085^{+0.038}_{-0.039}, \quad (95\% \text{ c.l.}) \\ \epsilon_2\epsilon_3 &= 0.061^{+0.046}_{-0.042}. \end{aligned} \quad (1)$$

When ϵ_3 is fixed to zero, they reduce to

$$\epsilon_1 < 0.011, \quad \epsilon_2 + 2.7\epsilon_1 = 0.040 \pm 0.026 \quad (95\% \text{ c.l.}) \quad (2)$$

3. Flat priors on combinations of the Taylor coefficients of the observable inflaton potential

The results of the last two subsections VC1, VC2 should be taken with a grain of salt for two reasons. First, when the running is large, the second slow-roll approximation is not necessarily accurate for all models allowed by the data, hence any relation between the spectral parameters $(\ln A_S, n_S, \alpha_S, r)$ and the underlying inflationary potential $V(\phi)$ includes a theoretical uncertainty. Second, for some spectra with a large running allowed by the data, there is no guarantee that there exists a single underlying inflationary model consistent with these spectra. Since all allowed models have $r \ll 1$, it is clear that they are consistent with the condition $\epsilon_1(k_*) \ll 1$ at the pivot scale, but on the edges of the observable range, they might be incompatible with $\epsilon_1(k) \leq 1$, i.e. with inflationary expansion.

In the method consisting in fitting directly the potential $V(\phi)$ with a numerical computation of the primordial spectra over the observable range, these caveats are avoided by construction. Still, one needs to make an

assumption concerning the shape of the inflaton potential in this range. In this subsection we assume that the observable inflaton potential can be approximated by a Taylor expansion of order either two or three. Our free parameters are the potential and its derivatives with respect to the inflaton field, evaluated when the pivot scale k_* crosses the Hubble radius during inflation: $V_0 = V$, $V_1 \equiv dV/d\phi$, $V_2 \equiv d^2V/d\phi^2$ and $V_3 \equiv d^3V/d\phi^3$. In order to avoid complicated parameter degeneracies, we impose flat priors on the combinations $(V_1/V_0)^2$, V_2/V_0 and V_3V_1/V_0^2 : these parameters are related linearly to the usual ‘potential slow-roll parameters’ and, although no slow-roll approximation is performed here, they remain not too far from linear combinations of (n_S, α_S, r) [68].

After running `CosmoMC`, for each model in our chains we can compute (n_S, α_S, r) defined at the pivot scale directly from the numerical primordial spectra. Hence, the results of this run can be readily compared in spectral parameter space with those of the previous subsection based on HFF parameters (like in [68, 78]). This comparison is illustrated in Figure 6. As expected, the run with $V_3 = 0$ leads to results very similar to those of the power-law model with $\alpha_S = 0$. The reason is that a quadratic potential cannot generate large running. This can be proved using the second-order slow-roll approximation, which remains accurate for all quadratic potentials compatible with the data. Following the same logic, one could expect the run with $V_3 \neq 0$ to mimic the results of the running model. This is far from being the case, as can be seen in Figure 6 when comparing the black and green contours. The model with cubic terms in the potential cannot not reach such large values of $|\alpha_S|$ and r as the running model. This can be understood in the following way. For models with large running and tensors, the Horizon Flow Functions $\epsilon_1(N_*)$ and $\epsilon_3(N_*)$ are not so small when the pivot scale crosses the Hubble radius, and the flow of equations leads $\epsilon_1(N)$ to reach order one even within the observable range. So, these models are not consistent with any underlying potential described by a third order polynomial within the observable range, even without assuming any extrapolation scheme beyond this range. The limit between consistent and inconsistent models depends crucially on the maximum wavenumber k_{\max} at which we require the primordial spectra to converge after Hubble crossing (see Appendix C and the discussion in [74]), in our case $k_{\max} = 5 \text{ Mpc}^{-1}$. For this value and under the assumption that the observable inflaton potential can be described by a third order polynomial, we find that $r < 0.15$ (at 95% c.l.), i.e. roughly the same bound as in the power-law model. At the same time we get $\alpha_S = -0.32 \pm 0.26$ (at 95% c.l.): negative running is still favored, but with twice smaller values of $|\alpha_S|$.

Note that the method of this subsection could be iterated at higher-order in the Taylor expansion of the observable inflaton. The results of [68] based on older data suggest that with a fourth-order expansion, the entire

range of (α_s, r) values allowed by the data in the running model could be compatible with the $V(\phi)$ model. However, this is at the expense of introducing a significant running of the running β_s (this parameter is governed by $d^4V/d\phi^4$ at the pivot scale). In that case the allowed ranges for (n_s, α_s, r) would be even larger than found in section VC1.

The results of the runs based on potential parameters and HFF parameters are also interesting to compare in the space of potential parameters $(V_1/V_0)^2$, V_2/V_0 and V_3V_1/V_0^2 . In order to perform such a comparison, we remapped the HFF parameters into potential slow-roll parameters using the formulae in Appendix B. The results are shown in Figure 7. Again, the power-law model and the second order expansion in $V(\phi)$ provide similar results, as can be seen from the two-dimensional likelihood contours in $((V_1/V_0)^2, V_2/V_0)$ space. For these models the best constrained combination is

$$\left[\frac{V_2}{V_0} - 1.9 \left(\frac{V_1}{V_0} \right)^2 \right] M_P^2 = -0.023 \pm 0.013, \quad (95\% \text{ c.l.}) \quad (3)$$

while

$$\left(\frac{V_1}{V_0} \right)^2 M_P^2 < 0.020. \quad (95\% \text{ c.l.}) \quad (4)$$

When the third derivative of the potential is turned on, the combination V_3V_1/V_0^2 is found to be in the range

$$\left(\frac{V_3V_1}{V_0^2} \right) M_P^4 = 0.017^{+0.015}_{-0.014}, \quad (95\% \text{ c.l.}) \quad (5)$$

while a reconstruction of the potential from spectral parameters (with running) would suggest a larger range

$$\left(\frac{V_3V_1}{V_0^2} \right) M_P^4 = 0.030^{+0.019}_{-0.018}. \quad (95\% \text{ c.l.}) \quad (6)$$

This discrepancy is equivalent to the one for α_s discussed above. For third-order polynomials $V(\phi)$, the upper bound on $(V_1/V_0)^2$ is the same as in Eq. (4) but the preferred combination of the first two parameter becomes

$$\left[\frac{V_2}{V_0} - 1.9 \left(\frac{V_1}{V_0} \right)^2 \right] M_P^2 = -0.041 \pm 0.021. \quad (95\% \text{ c.l.}) \quad (7)$$

VI. CONCLUSIONS

We have provided a detailed update on the present observational status of single-field inflation, paying particular attention to the robustness of our results to selection of data sets and theoretical uncertainties. WMAP5 data, in combination with the measurements of small scale CMB experiments and the halo power spectrum of luminous red galaxies from the SDSS data release 7

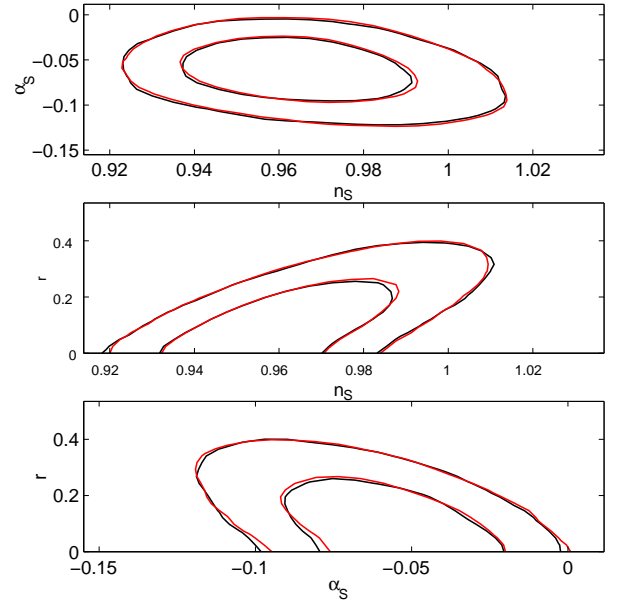


FIG. 4: Constraints from the CMB+LRG7 data set on combinations of the spectral parameters (n_s, α_s, r) . The black lines denote the constraints computed with the second-order slow-roll approximation, starting from flat priors on the HFF parameters at the pivot scale $(\epsilon_1, \epsilon_2, \epsilon_2\epsilon_3)$; the red lines denote the constraints obtained by using directly (n_s, r, α_s) , but enforcing the second-order consistency conditions for the tensor-to-scalar ratio and for the running of the tensor spectral index.

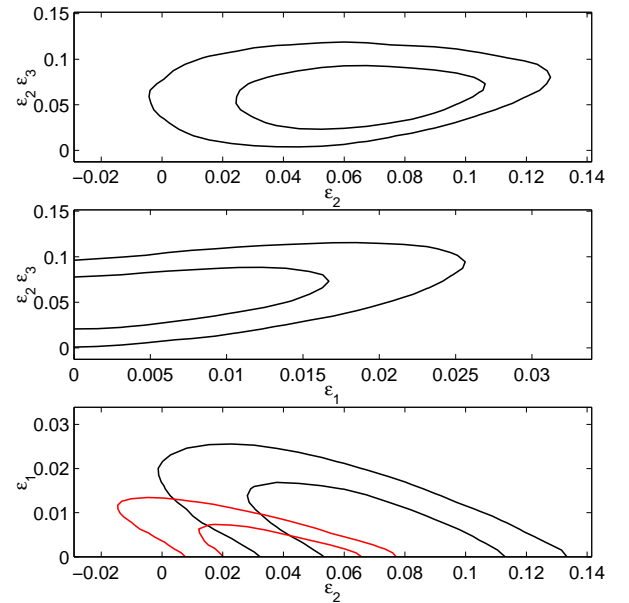


FIG. 5: Constraints from the CMB+LRG7 data set on combinations of the HFFs evaluated at the pivot scale $(\epsilon_1, \epsilon_2, \epsilon_2\epsilon_3)$ assuming: (red) $\epsilon_3 = 0$ and the first-order slow-roll approximation for the computation of the primordial spectra; (black) $\epsilon_3 \neq 0$ and the second-order slow-roll approximation.

	CMB only	CMB+LRG7	CMB+LRG7 ($r = 0$)
ω_b	$0.0221^{+0.0015}_{-0.0014}$	0.0219 ± 0.0012	0.0217 ± 0.0012
ω_c	$0.116^{+0.017}_{-0.016}$	$0.120^{+0.009}_{-0.008}$	$0.121^{+0.009}_{-0.008}$
h	$0.677^{+0.076}_{-0.070}$	$0.694^{+0.038}_{-0.030}$	$0.670^{+0.037}_{-0.035}$
τ	$0.101^{+0.041}_{-0.037}$	$0.097^{+0.040}_{-0.035}$	$0.093^{+0.038}_{-0.034}$
$\log [10^{10} A_s]$	3.17 ± 0.12	$3.18^{+0.09}_{-0.08}$	$3.18^{+0.09}_{-0.08}$
n_s	$0.972^{+0.045}_{-0.037}$	$0.964^{+0.039}_{-0.030}$	$0.949^{+0.026}_{-0.025}$
r	< 0.37	< 0.33	—
α_s	$-0.057^{+0.051}_{-0.054}$	$-0.063^{+0.061}_{-0.049}$	$-0.046^{+0.038}_{-0.039}$

TABLE III: Mean parameter values and bounds of the central 95%-credible intervals for the vanilla+ r + α_s and vanilla+ α_s parametrisations.

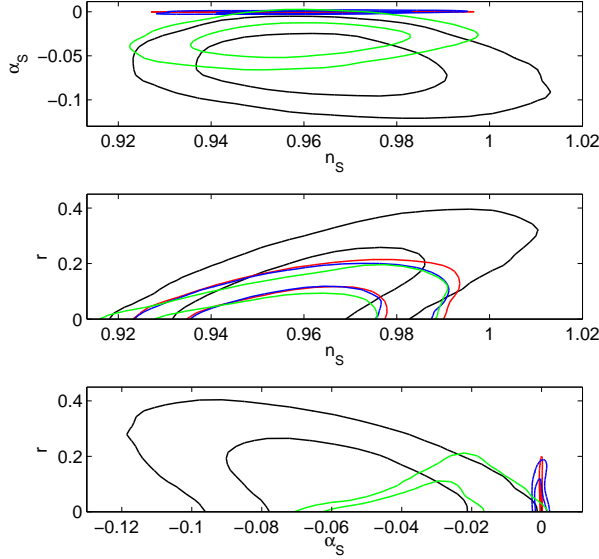


FIG. 6: Constraints from the CMB+LRG7 data set on combinations of the spectral parameters (n_s, α_s, r) under various assumptions: (blue) exact computation of the spectrum when the potential $V(\phi)$ is Taylor-expanded at order two in the observable range; (green) same with order three Taylor expansion; (black) spectrum computed with the second-order slow-roll approximation, starting from flat priors on the HFFs at the pivot scale ($\epsilon_1, \epsilon_2, \epsilon_3$); (red) same with $\epsilon_3 = 0$ prior (and first-order slow-roll approximation).

provide increasingly tight constraints on the physics of inflation.

We find that evidence against the Harrison-Zel'dovich spectrum is mounting, with a tilt of the spectrum now favoured at the level of about four standard deviations. Within the (n_s, r) -model which corresponds to most slow-roll inflation models, we infer constraints of $n_s = 0.962^{+0.028}_{-0.026}$ and $r < 0.17$ (at 95% confidence level), which puts, e.g., chaotic $\lambda\phi^4$ -inflation under severe pressure. Generally, the tendency of the data to prefer a convex shape of the inflaton potential has increased, though many concave models are still viable.

Tantalisingly, there remain mild indications that the data prefer a negative running of the spectral index at

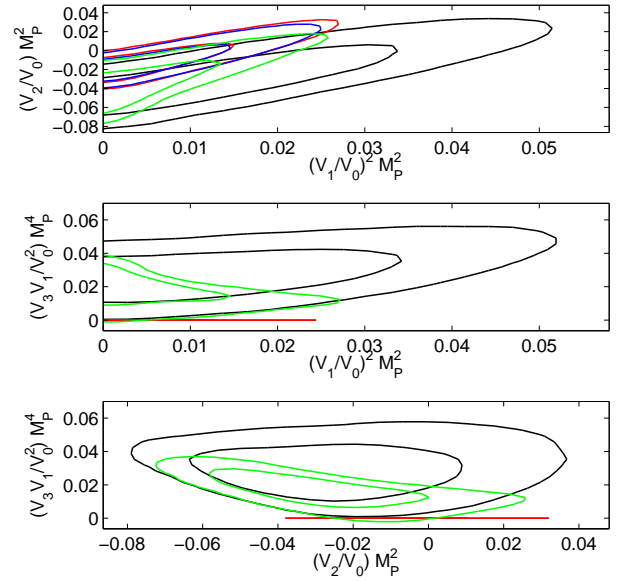


FIG. 7: Inflation constraints on combinations of the potential derivatives $V_1 \equiv dV/d\phi$, $V_2 \equiv d^2V/d\phi^2$, $V_3 \equiv d^3V/d\phi^3$ under various assumption: (blue) exact computation of the spectrum when the potential $V(\phi)$ is Taylor-expanded at order two in the observable range; (green) same with order three Taylor expansion; (black) spectrum computed with the second-order slow-roll approximation, starting from flat priors on the HFFs at the pivot scale ($\epsilon_1, \epsilon_2, \epsilon_3$), converted here into potential slow-roll parameters using exact formulae; (red) same with $\epsilon_3 = 0$ prior (and first-order slow-roll approximation). M_P stands for the reduced Planck mass.

roughly two standard deviations – indeed, a fair bit of allowed parameter space appears to be in conflict with the predictions of models with negligible fourth derivative of the potential in the observable range.

With a multitude of upcoming precise measurements of CMB polarisation and smaller scale CMB temperature perturbations by experiments like Planck, ACT, SPT, QUIET, SPIDER, PolarBear and EBEX, it is does not seem too optimistic to expect that we will soon be able to resolve these issues and take another big step towards reconstructing the physics that governed the inflationary era of the Universe.

Acknowledgments

We wish to thank Alberto Rubiño-Martín and Wessel Valkenburg for useful exchanges. We acknowledge the use of the Legacy Archive for Microwave Background Data Analysis (LAMBDA). Support for LAMBDA is provided by the NASA Office of Space Science. Numerical computations were performed on the CINECA BCX cluster under the INAF/CINECA agreement, the GRENDL cluster at the Centre for Scientific Computation Aarhus (CSC-AA), and the MUST cluster at LAPP (CNRS & Université de Savoie). FF thanks

the CERN Theory division for support. JH was supported by a Feodor Lynen-fellowship of the Alexander von Humboldt foundation. JL and JH acknowledge support from the EU 6th Framework Marie Curie Research and Training network “UniverseNet” (MRTN-CT-2006-035863). This research was partially supported by ASI contract I/016/07/0 ”COFIS”.

APPENDIX

We compare inflationary predictions with observations, by adopting a parametrisation of the primordial power spectra (PS henceforth) of curvature and tensor perturbations as:

$$\ln \frac{\mathcal{P}_X(k)}{\mathcal{P}_X(k_*)} = b_{0X} + b_{1X} \ln \left(\frac{k}{k_*} \right) + \frac{b_{2X}}{2} \ln^2 \left(\frac{k}{k_*} \right) \quad (8)$$

where $X = S, T$ stands for scalar and tensor, respectively, k_* is the pivot scale, $b_{1S} = n_S - 1$, $b_{1T} = n_T$, $b_{1S} = \alpha_S$, $b_{1T} = \alpha_T$.

A. Sampling the spectral parameters

In Section IV we have used the parametrisation of Eq. (8), sampling directly from the logarithm of $A_S (= \mathcal{P}_S(k_*)e^{b_{0S}})$, n_S and $r (= \mathcal{P}_T(k_*)e^{b_{0T}-b_{0S}}/\mathcal{P}_S(k_*))$, with $b_{2X} = 0$. The tensor spectral index has been fixed through the (first-order) consistency condition:

$$n_T = -\frac{r}{8}. \quad (9)$$

In Section V we have sampled A_S , n_S , r , α_S . The tensor spectral index has been fixed through the (second-order) consistency condition:

$$n_T = -\frac{r}{8} \left(2 - \frac{r}{8} - n_S \right). \quad (10)$$

The running of the tensor spectral index has been fixed to:

$$\alpha_T = \frac{r}{8} \left(\frac{r}{8} + n_S - 1 \right). \quad (11)$$

B. Sampling the Horizon Flow Functions (HFFs)

In Section V we have derived $\mathcal{P}_X(k_*)$, b_{iX} from the Hubble parameter H and the *horizon flow functions* ϵ_i (HFF henceforth) evaluated at the pivot scale k_* . The HFFs are defined as $\epsilon_1 = -\dot{H}/H^2$ and $\epsilon_{i+1} \equiv \dot{\epsilon}_i/(H\epsilon_i) = (d\epsilon_i/dN)/\epsilon_i$ with $i \geq 1$ and N the number of e -folds ($dN = Hdt$) [42]. The analytic slow-roll approximated power spectra has been obtained first through the Green’s function method (GFM henceforth)

in Refs. [43, 79]. The coefficients for the scalar spectrum are:

$$\begin{aligned} b_{S0} = & -2(C+1)\epsilon_1 - C\epsilon_2 + \left(-2C + \frac{\pi^2}{2} - 7\right)\epsilon_1^2 \\ & + \left(\frac{\pi^2}{8} - 1\right)\epsilon_2^2 + \left(-C^2 - 3C + \frac{7\pi^2}{12} - 7\right)\epsilon_1\epsilon_2 \\ & + \left(-\frac{1}{2}C^2 + \frac{\pi^2}{24}\right)\frac{d\epsilon_2}{dN} \end{aligned} \quad (12)$$

$$\begin{aligned} b_{S1} \equiv n_S - 1 = & -2\epsilon_1 - \epsilon_2 - 2\epsilon_1^2 - (2C+3)\epsilon_1\epsilon_2 - \\ & C\frac{d\epsilon_2}{dN} \end{aligned} \quad (13)$$

$$b_{S2} \equiv \alpha_S = -2\epsilon_1\epsilon_2 - \frac{d\epsilon_2}{dN}, \quad (14)$$

and for tensors are:

$$\begin{aligned} b_{T0} = & -2(C+1)\epsilon_1 + \left(-2C + \frac{\pi^2}{2} - 7\right)\epsilon_1^2 \\ & + \left(-C^2 - 2C + \frac{\pi^2}{12} - 2\right)\epsilon_1\epsilon_2, \end{aligned} \quad (15)$$

$$b_{T1} \equiv n_T = -2\epsilon_1 - 2\epsilon_1^2 - 2(C+1)\epsilon_1\epsilon_2, \quad (16)$$

$$b_{T2} \equiv \alpha_T = -2\epsilon_1\epsilon_2, \quad (17)$$

where $C \equiv \ln 2 + \gamma_E - 2 \approx -0.7296$ (γ_E is the Euler-Mascheroni constant) and $d\epsilon_2/dN = \epsilon_2\epsilon_3$. A similar structure has been obtained through the method of Comparison Equation [80].

For a Klein-Gordon scalar field ϕ , the potential V and its derivatives are related to H and ϵ_i as:

$$\begin{aligned} V = & 3M_P^2 H^2 \left(1 - \frac{\epsilon_1}{3}\right), \\ \frac{V_\phi^2 M_P^2}{V^2} = & 2\epsilon_1 \frac{\left(1 - \frac{\epsilon_1}{3} + \frac{\epsilon_2}{6}\right)^2}{\left(1 - \frac{\epsilon_1}{3}\right)^2}, \\ \frac{V_{\phi\phi} M_P^2}{V} = & \frac{2\epsilon_1 - \frac{\epsilon_2}{2} - \frac{2\epsilon_1^2}{3} + \frac{5\epsilon_1\epsilon_2}{6} - \frac{\epsilon_2^2}{12} - \frac{\epsilon_2\epsilon_3}{6}}{1 - \frac{\epsilon_1}{3}}, \\ \frac{V_{\phi\phi\phi} V_\phi M_P^4}{V^2} = & \frac{1 - \frac{\epsilon_1}{3} + \frac{\epsilon_2}{6}}{\left(1 - \frac{\epsilon_1}{3}\right)^2} \left(4\epsilon_1^2 - 3\epsilon_1\epsilon_2 + \frac{\epsilon_2\epsilon_3}{2}\right. \\ & + \epsilon_1^2\epsilon_2 - \epsilon_1\epsilon_2^2 - \frac{4}{3}\epsilon_1^3 - \frac{7}{6}\epsilon_1\epsilon_2\epsilon_3 \\ & \left. + \frac{\epsilon_2^2\epsilon_3}{6} + \frac{\epsilon_2\epsilon_3^2}{6} + \frac{\epsilon_2\epsilon_3\epsilon_4}{6}\right), \\ & \dots \end{aligned} \quad (18)$$

The use of the HFF parametrisation allows to reconstruct the derivatives of the potential without any additional approximation.

C. Sampling the potential parameters

In Section V we used the CosmoMC inflationary module⁵ released together with [68]. The basic principles of this

⁵ <http://www.lapp.in2p3.fr/~valkenbu/inflationH/>

module are the following.

In **CosmoMC**, the pivot scale is fixed once and for all, but different parameters defining the function $V(\phi - \phi_*)$ are passed to **CAMB** (here ϕ_* is the value of the inflaton field when the pivot scale crosses the Hubble radius; it does not need to be formulated explicitly). For each $V(\phi - \phi_*)$, the module computes the spectra $\mathcal{P}_S(k)$, $\mathcal{P}_T(k)$ within the range $[k_{\min}, k_{\max}] = [5 \times 10^{-6}, 5] \text{ Mpc}^{-1}$ needed by **CAMB**, imposing that $aH = k_*$ when $\phi = \phi_*$. So, the code first finds the inflationary attractor solution around $\phi = \phi_*$, computes H_* and normalizes the scale factor so that $a_* = k_*/H_*$. Then, each mode is integrated numerically for k/aH varying between two adjustable ratios: here, 50 and $1/50$. The evolution of each scalar/tensor mode is given by

$$\frac{d^2 \xi_{S,T}}{d\eta^2} + \left[k^2 - \frac{1}{z_{S,T}} \frac{d^2 z_{S,T}}{d\eta^2} \right] \xi_{S,T} = 0 \quad (19)$$

with $\eta = \int dt/a(t)$ and $z_S = a\dot{\phi}/H$ for scalars, $z_T = a$ for tensors. The code integrates this equation starting from the initial condition $\xi_{S,T} = e^{-ik\eta}/\sqrt{2k}$ when $k/aH = 50$, and computes

$$\mathcal{P}_S = \lim_{k \ll aH} \frac{k^3}{2\pi^2} \frac{|\xi_S|^2}{z_S^2}, \quad \mathcal{P}_T = \lim_{k \ll aH} \frac{32k^3}{\pi m_P^2} \frac{|\xi_T|^2}{z_T^2}. \quad (20)$$

So, the earliest (latest) time considered in the code is that when $k_{\min}/aH = 50$ ($k_{\max}/aH = 1/50$), which in the attractor solution uniquely determines extreme values of $(\phi - \phi_*)$ according to some potential. In the module this is translated to demanding that aH grows according to the aforementioned ratios: by $50k_*/k_{\min}$ before $\phi = \phi_*$, and by $50k_{\max}/k_*$ afterwards. Hence, one of the preliminary tasks of the module is to find the earliest time. If by then, a unique attractor solution for the background field cannot be found within a given accuracy (10% for $\dot{\phi}_{\text{ini}}$), the model is rejected. So, the module implicitly assumes that inflation starts at least a few e -folds before the present Hubble scale exits the horizon (this assumption is relaxed in the second version of the module based on $H(\phi)$ reconstruction [72]). In addition, the module imposes a positive, monotonic potential and an accelerating scale factor during the period of interest. As a result of the chosen method, the potential is slightly extrapolated beyond the observable window, in order to reach the mentioned conditions for the beginning and ending of the numerical integration. The range of extrapolation is still very small in comparison with an extrapolation over the full duration of inflation after the observable modes have exited the Hubble radius. Note that in this approach one does not need to make any assumption about reheating and the duration of the radiation era.

-
- [1] A. A. Starobinsky, Phys. Lett. **B91**, 99 (1980).
 - [2] A. H. Guth, Phys. Rev. **D23**, 347 (1981).
 - [3] G. Hinshaw, J. L. Weiland, R. S. Hill, N. Odegard, D. Larson, C. L. Bennett, J. Dunkley, B. Gold, M. R. Greason, N. Jarosik, et al., ApJS **180**, 225 (2009), 0803.0732.
 - [4] E. Komatsu et al. (WMAP), Astrophys. J. Suppl. **180**, 330 (2009), 0803.0547.
 - [5] H. V. Peiris and R. Easther, JCAP **0807**, 024 (2008), 0805.2154.
 - [6] W. H. Kinney, E. W. Kolb, A. Melchiorri, and A. Riotto, Phys. Rev. **D78**, 087302 (2008), 0805.2966.
 - [7] C. L. Reichardt, P. A. R. Ade, J. J. Bock, J. R. Bond, J. A. Brevik, C. R. Contaldi, M. D. Daub, J. T. Dempsey, J. H. Goldstein, W. L. Holzapfel, et al., Astrophys. J. **694**, 1200 (2009), 0801.1491.
 - [8] W. J. Percival et al., Mon. Not. Roy. Astron. Soc. **381**, 1053 (2007), 0705.3323.
 - [9] P. Astier et al. (The SNLS), Astron. Astrophys. **447**, 31 (2006), astro-ph/0510447.
 - [10] H. C. Chiang, P. A. R. Ade, D. Barkats, J. O. Battle, E. M. Bierman, J. J. Bock, C. D. Dowell, L. Duband, E. F. Hivon, W. L. Holzapfel, et al., ArXiv e-prints (2009), 0906.1181.
 - [11] QUaD collaboration: M. L. Brown, P. Ade, J. Bock, M. Bowden, G. Cahill, P. G. Castro, S. Church, T. Culverhouse, R. B. Friedman, K. Ganga, et al., ArXiv e-prints (2009), 0906.1003.
 - [12] R. Kessler et al., Astrophys. J. Suppl. **185**, 32 (2009), 0908.4274.
 - [13] (2006), astro-ph/0604069.
 - [14] A. D. Hincks, V. Acquaviva, P. Ade, P. Aguirre, M. Amiri, J. W. Appel, L. F. Barrientos, E. S. Battistelli, J. R. Bond, B. Brown, et al., ArXiv e-prints (2009), 0907.0461.
 - [15] J. Ruhl, P. A. R. Ade, J. E. Carlstrom, H. Cho, T. Crawford, M. Dobbs, C. H. Greer, N. W. Halverson, W. L. Holzapfel, T. M. Lanting, et al., in *Society of Photo-Optical Instrumentation Engineers (SPIE) Conference Series*, edited by C. M. Bradford, P. A. R. Ade, J. E. Aguirre, J. J. Bock, M. Dragovan, L. Duband, L. Earle, J. Glenn, H. Matsuhara, B. J. Naylor, H. T. Nguyen, M. Yun, & J. Zmuidzinas (2004), vol. 5498 of *Society of Photo-Optical Instrumentation Engineers (SPIE) Conference Series*, pp. 11–29.
 - [16] D. Samtleben and for the QUIET collaboration, ArXiv e-prints (2008), 0806.4334.
 - [17] B. P. Crill, P. A. R. Ade, E. S. Battistelli, S. Benton, R. Bihary, J. J. Bock, J. R. Bond, J. Brevik, S. Bryan, C. R. Contaldi, et al., in *Society of Photo-Optical Instrumentation Engineers (SPIE) Conference Series* (2008), vol. 7010 of *Society of Photo-Optical Instrumentation Engineers (SPIE) Conference Series*.
 - [18] A. T. Lee, H. Tran, P. Ade, K. Arnold, J. Borrill, M. A. Dobbs, J. Errard, N. Halverson, W. L. Holzapfel, J. Howard, et al., in *American Institute of Physics Conference Series*, edited by H. Kodama & K. Ioka (2008), vol. 1040 of *American Institute of Physics Conference*

Series, pp. 66–77.

- [19] P. Oxley, P. A. Ade, C. Baccigalupi, P. deBernardis, H. Cho, M. J. Devlin, S. Hanany, B. R. Johnson, T. Jones, A. T. Lee, et al., in *Society of Photo-Optical Instrumentation Engineers (SPIE) Conference Series*, edited by M. Strojnik (2004), vol. 5543 of *Society of Photo-Optical Instrumentation Engineers (SPIE) Conference Series*, pp. 320–331.
- [20] M. R. Nolta, J. Dunkley, R. S. Hill, G. Hinshaw, E. Komatsu, D. Larson, L. Page, D. N. Spergel, C. L. Bennett, B. Gold, et al., *ApJS* **180**, 296 (2009), 0803.0593.
- [21] J. Dunkley, E. Komatsu, M. R. Nolta, D. N. Spergel, D. Larson, G. Hinshaw, L. Page, C. L. Bennett, B. Gold, N. Jarosik, et al., *ApJS* **180**, 306 (2009), 0803.0586.
- [22] B. A. Reid, W. J. Percival, D. J. Eisenstein, L. Verde, D. N. Spergel, R. A. Skibba, N. A. Bahcall, T. Budavari, M. Fukugita, J. R. Gott, et al., *ArXiv e-prints* (2009), 0907.1659.
- [23] B. A. Reid, D. N. Spergel, and P. Bode, *Astrophys. J.* **702**, 249 (2009), 0811.1025.
- [24] A. G. Riess, L. Macri, S. Casertano, M. Sosey, H. Lampeitl, H. C. Ferguson, A. V. Filippenko, S. W. Jha, W. Li, R. Chornock, et al., *Astrophys. J.* **699**, 539 (2009), 0905.0695.
- [25] A. Lewis and S. Bridle, *Phys. Rev. D* **66**, 103511 (2002), *arXiv:astro-ph/0205436*.
- [26] A. Lewis, A. Challinor, and A. Lasenby, *Astrophys. J.* **538**, 473 (2000), *arXiv:astro-ph/9911177*.
- [27] M. Cortès, A. R. Liddle, and P. Mukherjee, *Phys. Rev. D* **75**, 083520 (2007), *arXiv:astro-ph/0702170*.
- [28] D. J. Fixsen, *ArXiv e-prints* (2009), 0911.1955.
- [29] K. Ichikawa, T. Sekiguchi, and T. Takahashi, *Phys. Rev. D* **78**, 043509 (2008), 0712.4327.
- [30] J. Hamann, J. Lesgourgues, and G. Mangano, *JCAP* **3**, 4 (2008), 0712.2826.
- [31] E. Komatsu and U. Seljak, *MNRAS* **336**, 1256 (2002), *arXiv:astro-ph/0205468*.
- [32] W. K. Hastings, *Biometrika* **57**(1), 97 (1970).
- [33] A. Gelman and D. B. Rubin, *Statistical Science* **7**, 457 (1992).
- [34] E. R. Harrison, *Phys. Rev. D* **1**, 2726 (1970).
- [35] Y. B. Zeldovich, *MNRAS* **160**, 1P (1972).
- [36] P. J. E. Peebles and J. T. Yu, *Astrophys. J.* **162**, 815 (1970).
- [37] M. Kawasaki and T. Sekiguchi, *ArXiv e-prints* (2009), 0911.5191.
- [38] H. V. Peiris and L. Verde (2009), 0912.0268.
- [39] M. Pettini, B. J. Zych, M. T. Murphy, A. Lewis, and C. C. Steidel, *MNRAS* **391**, 1499 (2008), 0805.0594.
- [40] F. Iocco, G. Mangano, G. Miele, O. Pisanti, and P. D. Serpico, *Phys. Rep.* **472**, 1 (2009), 0809.0631.
- [41] G. W. Pratt, J. H. Croston, M. Arnaud, and H. Böhringer, *A&A* **498**, 361 (2009), 0809.3784.
- [42] D. J. Schwarz, C. A. Terrero-Escalante, and A. A. Garcia, *Phys. Lett. B* **517**, 243 (2001), *astro-ph/0106020*.
- [43] S. M. Leach, A. R. Liddle, J. Martin, and D. J. Schwarz, *Phys. Rev. D* **66**, 023515 (2002), *astro-ph/0202094*.
- [44] W. H. Kinney, *Phys. Rev. D* **66**, 083508 (2002), *astro-ph/0206032*.
- [45] A. Makarov, *Phys. Rev. D* **72**, 083517 (2005), *astro-ph/0506326*.
- [46] R. Easther and H. Peiris, *JCAP* **0609**, 010 (2006), *astro-ph/0604214*.
- [47] G. Ballesteros, J. A. Casas, and J. R. Espinosa, *JCAP* **0603**, 001 (2006), *hep-ph/0601134*.
- [48] G. Ballesteros, J. A. Casas, J. R. Espinosa, R. Ruiz de Austri, and R. Trotta, *JCAP* **0803**, 018 (2008), 0711.3436.
- [49] W. Valkenburg, L. M. Krauss, and J. Hamann, *Phys. Rev. D* **78**, 063521 (2008), 0804.3390.
- [50] K. Freese, J. A. Frieman, and A. V. Olinto, *Physical Review Letters* **65**, 3233 (1990).
- [51] G. R. Dvali, Q. Shafi, and R. K. Schaefer, *Phys. Rev. Lett.* **73**, 1886 (1994), *hep-ph/9406319*.
- [52] F. Bezrukov and M. Shaposhnikov, *JHEP* **07**, 089 (2009), 0904.1537.
- [53] A. D. Linde, *Phys. Lett. B* **129**, 177 (1983).
- [54] A. R. Liddle and S. M. Leach, *Phys. Rev. D* **68**, 103503 (2003), *astro-ph/0305263*.
- [55] F. Lucchin and S. Matarrese, *Phys. Rev. D* **32**, 1316 (1985).
- [56] D. H. Lyth and A. Riotto, *Phys. Rept.* **314**, 1 (1999), *hep-ph/9807278*.
- [57] W. J. Percival, B. A. Reid, D. J. Eisenstein, N. A. Bahcall, T. Budavari, J. A. Frieman, M. Fukugita, J. E. Gunn, Z. Ivezic, G. R. Knapp, et al., *ArXiv e-prints* (2009), 0907.1660.
- [58] J. Hamann, S. Hannestad, M. S. Sloth, and Y. Y. Y. Wong, *Phys. Rev. D* **75**, 023522 (2007), *arXiv:astro-ph/0611582*.
- [59] B. A. Reid, L. Verde, R. Jimenez, and O. Mena, *ArXiv e-prints* (2009), 0910.0008.
- [60] S. Seager, D. D. Sasselov, and D. Scott, *Astrophys. J.* **523**, L1 (1999), *arXiv:astro-ph/9909275*.
- [61] S. Seager, D. D. Sasselov, and D. Scott, *ApJS* **128**, 407 (2000), *arXiv:astro-ph/9912182*.
- [62] W. Y. Wong, A. Moss, and D. Scott, *MNRAS* **386**, 1023 (2008), 0711.1357.
- [63] D. Scott and A. Moss, *MNRAS* **397**, 445 (2009), 0902.3438.
- [64] J. A. Rubino-Martin, J. Chluba, W. A. Fendt, and B. D. Wandelt, *ArXiv e-prints* (2009), 0910.4383.
- [65] D. Grin and C. M. Hirata, *ArXiv e-prints* (2009), 0911.1359.
- [66] W. A. Fendt, J. Chluba, J. A. Rubiño-Martín, and B. D. Wandelt, *ApJS* **181**, 627 (2009), 0807.2577.
- [67] J. A. Adams, G. G. Ross, and S. Sarkar, *Nucl. Phys. B* **503**, 405 (1997), *hep-ph/9704286*.
- [68] J. Lesgourgues and W. Valkenburg, *Phys. Rev. D* **75**, 123519 (2007), *arXiv:astro-ph/0703625*.
- [69] W. H. Kinney, E. W. Kolb, A. Melchiorri, and A. Riotto, *Phys. Rev. D* **74**, 023502 (2006), *astro-ph/0605338*.
- [70] H. Peiris and R. Easther, *JCAP* **0607**, 002 (2006), *astro-ph/0603587*.
- [71] H. Peiris and R. Easther, *JCAP* **0610**, 017 (2006), *astro-ph/0609003*.
- [72] J. Lesgourgues, A. A. Starobinsky, and W. Valkenburg, *JCAP* **0801**, 010 (2008), 0710.1630.
- [73] B. A. Powell and W. H. Kinney, *JCAP* **0708**, 006 (2007), 0706.1982.
- [74] J. Hamann, J. Lesgourgues, and W. Valkenburg, *JCAP* **0804**, 016 (2008), 0802.0505.
- [75] S. M. Leach and A. R. Liddle, *Phys. Rev. D* **68**, 123508 (2003), *astro-ph/0306305*.
- [76] J. Martin and C. Ringeval, *JCAP* **8**, 9 (2006), *arXiv:astro-ph/0605367*.
- [77] F. Finelli, M. Rianna, and N. Mandolesi, *JCAP* **0612**, 006 (2006), *astro-ph/0608277*.

- [78] P. Adshead and R. Easther, JCAP **10**, 47 (2008), 0802.3898.
- [79] J.-O. Gong and E. D. Stewart, Phys. Lett. **B510**, 1 (2001), astro-ph/0101225.
- [80] R. Casadio, F. Finelli, A. Kamenshchik, M. Luzzi, and G. Venturi, JCAP **0604**, 011 (2006), gr-qc/0603026.